Supplementary Materials

The EDS Mapping Images of Devices

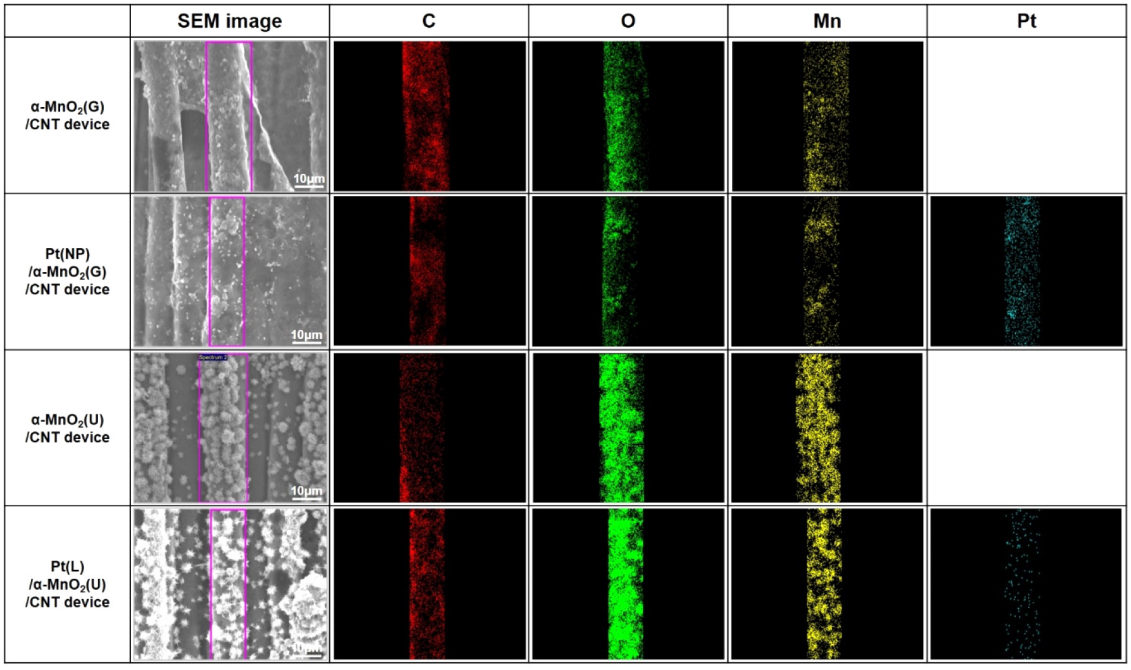

Fig. S1. EDS images of each C, Mn, O, and Pt element of each fabricated thermal catalytic device.

The EDS mapping image of each specimen was measured using field emission scanning electron microscopy (FE-SEM, JSM-6701F, JEOL Ltd.), and Energy dispersive spectroscopy (EDS, INCA, Oxford Instruments Ltd.) and is shown in Fig. S1. All nanostructures fabricated on the CNT devices are mainly composed of Mn and O elements. Both Pt elements of Pt/α-MnO_2/CNT devices are mainly detected on the surface of the α-MnO_2 nanostructures as shown in the EDS mapping images. Since the Pt element was detected in a small amount in EDS mapping, XPS was used to measure the crystallinity of the Pt element of the specimen. XPS results are described in the manuscript (see Fig. 5).

The EDS Mapping Images of the Pt(NP)/CNT Device and Its Thermal Catalytic Characteristic

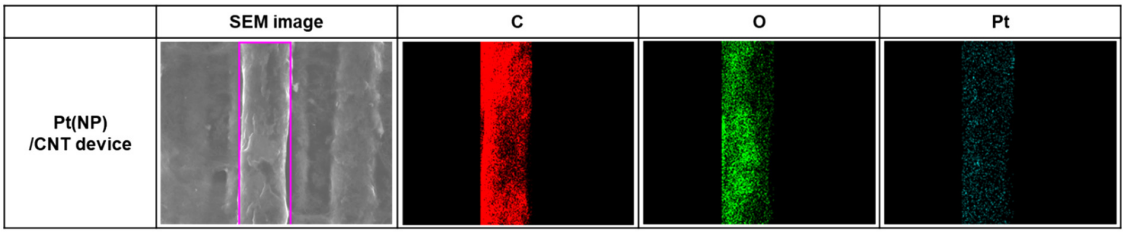

Fig. S2. EDS images of each C, Mn, O, and Pt element of the Pt(NP)/CNT device.

Table S1. Normalized toluene concentration of gaseous toluene after catalytic oxidation and operating energy consumption associated with each device under (a) direct and (b) indirect heating conditions (data of Fig. 6)

(a) Direct Heating Conditions	CNT element	α-MnO_2(G) /CNT device	Pt(NP) /α-MnO_2(G) /CNT device	α-MnO_2(U) /CNT device	Pt(L) /α-MnO_2(U) /CNT device	Pt(NP) /CNT device
Normalized toluene Concentration [C/C0]	0.613 (0.049)	0.569 (0.199)	0.397 (0.049)	0.563 (0.178)	0.365 (0.043)	0.514 (0.052)
Energy consumption [kJ]	9.676 (1.515)	9.357 (2.053)	10.539 (1.651)	7.919 (1.706)	9.658 (0.730)	8.459 (0.466)
(b) Indirect Heating Conditions	**CNT element**	**α-MnO_2(G) /CNT device**	**Pt(NP)/α-MnO_2(G) /CNT device**	**α-MnO_2(U) /CNT device**	**Pt(L)/α-MnO_2(U) /CNT device**	**Pt(NP) /CNT device**
Normalized toluene Concentration [C/C0]	0.657 (0.051)	0.645 (0.087)	0.627 (0.028)	0.616 (0.019)	0.570 (0.038)	0.622 (0.018)
Energy consumption [kJ]	1849.580	1849.580	1849.580	1849.580	1849.580	1849.580

The Pt(NP)/CNT device has been fabricated by using the same fabrication process as mentioned in 2. Experimental section. The EDS mapping image of the Pt(NP)/CNT device was shown in Fig. S2. The Pt element is mainly detected on the surface of the CNT device as shown in the EDS mapping image.

It is difficult to compare the catalytic behavior of each sample because the amount of Pt is very small and not the same as that of MnO_2. However, the catalytic behavior of Pt(NP)/CNT-coated glass-fiber textile specimen was higher under the direct heating condition than under the indirect heating condition as shown in Table S1. Under direct heating conditions, the thermal catalytic device featuring Pt(NP)/CNT-coated glass-fiber textile achieves higher toluene decomposition efficiency than α-MnO_2/CNT-coated glass-fiber textiles and lower toluene decomposition efficiency than Pt decorated α-MnO_2/CNT-coated glass-fiber textiles. Under indirect heating conditions, the Pt(NP)/CNT-coated glass-fiber textile shows almost similar catalytic behavior to α-MnO_2/CNT-coated glass-fiber textiles.

The catalytic activities of pristine MnO_2 structures and MnO_2 structures combined with noble metal structures were represented in Table S2. Comparing the performance of the catalysts described in the literature to our study under identical conditions is difficult, because the amount of catalyst used in the catalytic device in our study is too small (0.002g). However, Pt(L)/α-MnO_2(U)/CNT-coated glass-fiber textile shows relatively high WHSV, which value was calculated by assuming that the closed chamber used in evaluating the toluene decomposition efficiency in this study is the open chamber with a flow rate.

Table S2. Comparison of the catalytic activity of MnO2 structures for decomposing toluene

Catalyst type	VOC type	VOC cons. (ppm)	Toluene oxidation activity (℃)	Weight of catalyst (g)	Toluene conversion (%)	WHSV (mlg-1h-1)	Reactor inner diameter (mm)	Ref.
Ag/MnO_2	Toluene	1000	212	0.200	90	20000		[1]
α-MnO_2	Toluene		237	0.300	90	10000	9	[2]
γ-MnO_2	Toluene	1000	251	0.100	90	60000	6	[3]
α-MnO_2@ Co_3O_4	Toluene	1000	229	0.100	90	48000	6	[4]
Pt/MnO_2	Toluene	1500	205	0.090	90	60000	10	[5]
Pt(L)/α-MnO_2 (U)/CNT	Toluene	50-60	215	0.002	65.1	195000	44	Present work

Measurement of the Surface Roughness of Catalysts

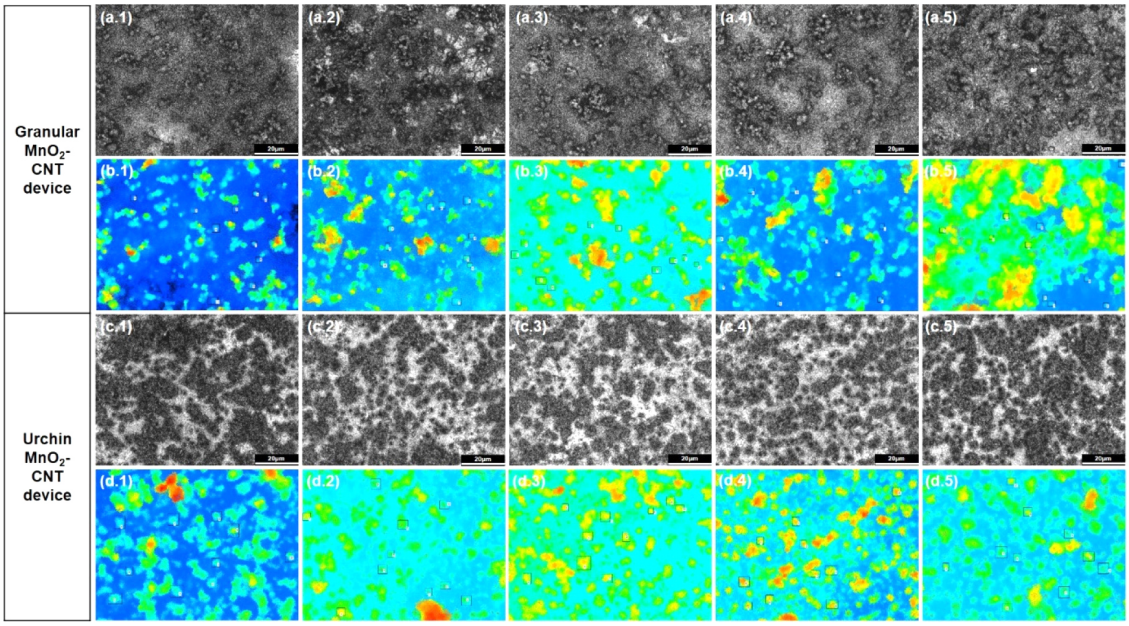

Fig. S3. The optical and surface profile images of (a.1-5) (b.1-5) granular MnO_2 nanostructures, and (c.1-5) (d.1-5) urchin-MnO_2 nanostructures.

Each MnO_2 nanostructure was synthesized on the polished Si substrate, and roughness was measured using a laser scanning confocal microscope (VK-X1050, KEYENCE Ltd., Japan). Fig. S3 a-b and c-d represent the optical and surface profile images of granular and urchin-MnO_2 nanostructures, respectively. 50 MnO_2 nanostructures on the surface of each specimen were randomly selected, and each average roughness (R_a) was measured. The average R_a values (standard deviations) of granular and urchin-MnO_2 nanostructures are 0.59 (±0.17) and 1.08 (±0.20) μm, respectively. The urchin-MnO_2 nanostructure exhibits higher roughness than granular-MnO_2 nanostructure and therefore has a higher specific surface area per equal area.

Measurement of the electrical resistance of devices

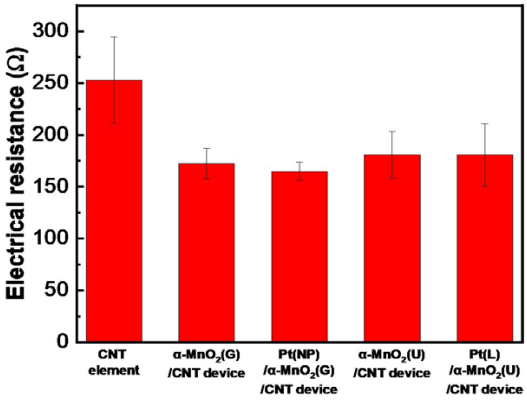

Fig. S4. The electrical resistance of various devices.

Electrodes were attached to two edges of various specimens (CNT-coated (CNT element), α-MnO_2(G)/CNT-coated, Pt(NP)/α-MnO_2(G)/CNT-coated, α-MnO_2(U)/CNT-coated, and Pt(L)/α-MnO_2(U)/CNT-coated glass-fiber textile specimens) as described in the experimental section. The electrical resistance of each specimen was measured using an electrometer (GDM-8351. Good Will Instrument Co., Ltd.) and is shown in Fig. S4. The electrical resistance of the CNT-coated glass-fiber textile was measured to be 253.00 Ω. The electrical resistances of α-MnO_2(G)/CNT-coated, Pt(NP)/α-MnO_2(G)/CNT-coated, α-MnO_2(U)/CNT-coated and Pt(L)/α-MnO_2(U)/CNT-coated glass-fiber textiles are 172.50, 164.75, 181.00, and 180.75 Ω, respectively. The electrical resistance of the CNT-coated glass-fiber textile decreases slightly after the deposition of α-MnO_2 nanostructures and the subsequent deposition of Pt nanostructures owing to the curing of uncured binder in the CNT layer during the thermal processing of the α-MnO_2 and Pt nanostructures.

Direct and Indirect Heating Processes

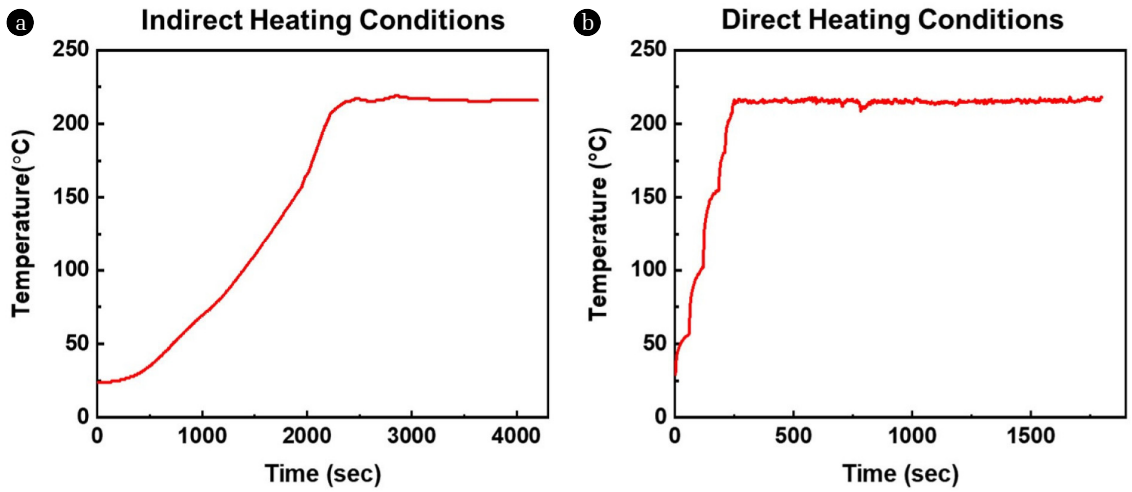

Fig. S5. Change in the temperature of the CNT element as a function of operating time under (a) indirect and (b) direct heating conditions.

In this study, the toluene decomposition efficiencies of thermal catalytic devices were evaluated at 215 °C. Direct and indirect heating processes were used to attain and maintain this temperature. Each heating process is described in the experimental section. The temperature of a thermal catalytic device operated under indirect heating conditions was measured using a thermometer (DE-305, PATOS Co.) and K-type thermocouple (EQ-TC-K-Cali-18S-LD, MTI Korea Co.) inserted into the quartz chamber. Whereas the temperature of the same thermal catalytic device operated under direct heating conditions was measured using a thermometer (midi Logger GL220, Graphtec Co.) and a K-type thermocouple (SEN-120, SENTECH ENG Inc.) attached to the surface of the thermal catalytic device.

A commercial furnace was used in the indirect heating process; during this process, the temperature was increased to 215 °C at a programmed rate of 5 °C/min (duration of ~40 min) and maintained for 30 min. The total operating time and energy consumption of the indirect heating process were approximately 70 min and 1849.580 kJ, respectively. The programmed heating rate of the indirect heating process of 5 °C/min exceeds that of the direct heating process of 15 °C/min. This is because the measured heating rate is less than the programmed heating rate during the indirect heating process.

In the direct heating process, the thermal catalytic device was directly connected to the power supply. The temperature was increased stepwise over 5 min at an average heating rate of 15 °C/min to 215 °C, and maintained for 30 min. The total operating time and energy consumption of the direct heating process were approximately 35 min and 5.019 kJ, respectively.

Before and After Five Toluene Decomposition Processes

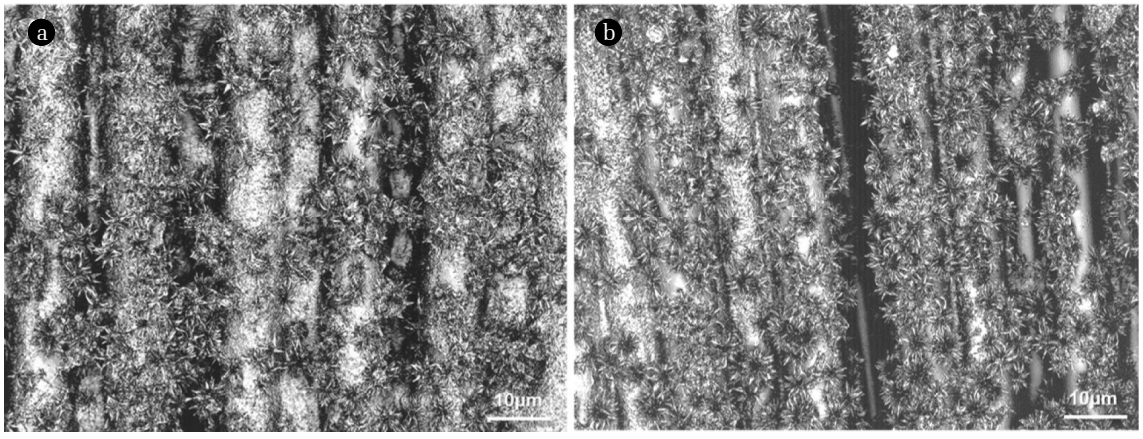

Fig. S6. Laser microscope images of the Pt(L)/MnO_2(U)/CNT devices, which were conducted (a) before, and (b) after five toluene decomposition processes.

The surface morphologies of Pt(L)/MnO_2(U)/CNT device before and after five toluene decomposition processes were observed by using a laser microscope (VK-X1050, KEYENCE Corp). Both devices were fabricated in the same batch. Structural deformation on the device after repeated toluene decomposition experiments was not observed as shown in Fig. S6 (b).

Reference

1. Li J, Qu Z, Qin Y, Wang H. Effect of MnO_2 morphology on the catalytic oxidation of toluene over Ag/MnO_2 catalysts. *Appl. Surf. Sci.* 2016;385:234–240. https://doi.org/10.1016/j.apsusc.2016.05.114.
2. Cheng G, Yu L, Lan B, et al. Controlled synthesis of α-MnO_2 nanowires and their catalytic performance for toluene combustion. *Mater. Res. Bull.* 2016;75:17–24. https://doi.org/10.1016/j.materresbull.2015.11.017.
3. Liu L, Li J, Zhang H, et al. In situ fabrication of highly active γ-MnO_2/$SmMnO_3$ catalyst for deep catalytic oxidation of gaseous benzene, ethylbenzene, toluene, and o-xylene. *J. Hazard. Mater.* 2019;362:178–186. https://doi.org/10.1016/j.jhazmat.2018.09.012.
4. Ren Q, Mo S, Fan J, et al. Enhancing catalytic toluene oxidation over MnO_2@Co_3O_4 by constructing a coupled interface. *Chinese J. Catal.* 2020;41:1873–1883. https://doi.org/10.1016/S1872-2067(20)63641-5.
5. Hu J, Gao X, Fan Q, Gao X. Facial controlled synthesis of Pt/MnO_2 catalysts with high efficiency for VOCs combustion. *RSC Adv.* 2021;11:16547–16556. https://doi.org/10.1039/d1ra02112e.